A Calibration Method for Nanowire Biosensors to Suppress Device-to-device Variation

Fumiaki N. Ishikawa[a], **Marco Curreli**[b], **Hsiao-Kang Chang**[a], **Po-Chiang Chen**[a], **Rui Zhang**[b], **Richard J. Cote**[c], **Mark E. Thompson**[b], and **Chongwu Zhou**[a,*]

[a] Department of Electrical Engineering, University of Southern California, Los Angeles, CA 90089

[b] Department of Chemistry, University of Southern California, Los Angeles, CA 90089

[c] Department of Pathology, University of Southern California, Los Angeles, CA 90089

Abstract

Nanowire/nanotube biosensors have stimulated significant interest; however the inevitable device-to-device variation in the biosensor performance remains a great challenge. We have developed an analytical method to calibrate nanowire biosensor responses that can suppress the device-to-device variation in sensing response significantly. The method is based on our discovery of a strong correlation between the biosensor gate dependence (dI_{ds}/dV_g) and the absolute response (absolute change in current, ΔI). In_2O_3 nanowire based biosensors for streptavidin detection were used as the model system. Studying the liquid gate effect and ionic concentration dependence of strepavidin sensing indicates that electrostatic interaction is the dominant mechanism for sensing response. Based on this sensing mechanism and transistor physics, a linear correlation between the absolute sensor response (ΔI) and the gate dependence (dI_{ds}/dV_g) is predicted and confirmed experimentally. Using this correlation, a calibration method was developed where the absolute response is divided by dI_{ds}/dV_g for each device, and the calibrated responses from different devices behaved almost identically. Compared to the common normalization method (normalization of the conductance/resistance/current by the initial value), this calibration method was proved advantageous using a conventional transistor model. The method presented here substantially suppresses device-to-device variation, allowing the use of nanosensors in large arrays.

Keywords

Nanowire; nanobiosensor; calibration method; sensing mechanism

Introduction

Biological sensors based on nanowire/nanotube field effect transistors (FETs) are one of the most promising applications of bionanotechnology. As a proof of their promising capabilities, nanowire/nanotube sensors have been used to detect a large variety of biological molecules, ranging from proteins to nucleotide sequences;[1–15] to monitor enzymatic activities;[16] and to observe cellular signaling/responses,[17–19] with sensitivity and response time comparable or better than conventional techniques (ELISA). An important challenge holding back the

practical application of nanobiosensors to bio-analytical measurements is the device-to-device variation in the device properties such as conductance, threshold voltage, and transconductance. This variation exists between devices on different substrates as well as between devices within an array on a single substrate.[20, 21] This results in unreliable detection, making quantitative analysis difficult. This challenge must be addressed to bridge the gap between academic research and practical use of the technology.

While effort has been devoted to the fabrication of more uniform devices,[5, 9, 22–40] there have been few reports tackling the problem with a data analysis approach. Recently it was reported that the Langmuir isotherm model can be used to calibrate the sensor performance of carbon nanotube biosensors.[41] While this method is effective in reducing response discrepancies, it requires testing of several different analyte concentrations for each device to use Langmuir fitting, developing a unique calibration curve for each device. We report herein an analytical method to calibrate nanowire biosensors, which gives significantly suppressed device-to-device variation in sensing response. We use the correlation between the biosensor gate dependence and the absolute responses (absolute change in current, ΔI) as the basis of the calibration method. In_2O_3 nanowire FET based biosensors for streptavidin were used as a model system, to demonstrate that an electrostatic interaction is the dominant sensing mechanism. We developed a calibration method involving dividing the absolute response by dI_{ds}/dV_g for each device, which markedly improved the device-to-device variation, as verified by the much reduced coefficient of variance (CV) from 59% for the absolute response to 25% for the calibrated response, respectively. The superiority of this calibration method to the common normalization method is shown mathematically using a conventional transistor model, and experimentally confirmed. Our method is a significant step forward toward the broader application of nanowire biosensors.

Results and Discussion

Variation of as-made biosensors

Our sensing devices based on indium oxide nanowires were fabricated following a previously developed procedure.[4, 42, 43] The only deviation from this procedure is a novel design of interdigitated source and drain electrodes that resulted in high yield (Figure 1a–c). Details of the fabrication are in the method section. We note that this procedure allows inexpensive and scalable fabrication with an uniformity similar to the one obtained with an aid of Langmuir-Blodgett assembly.[20] The uniformity of our device in terms of threshold voltage is shown in Figure S1. Figure 1a shows the photograph of a complete 3″ wafer with multiple biosensor chips. Figure 1b shows one of the chips and the inset displays a typical device with interdigitated electrodes, which serve to increase the effective channel width and subsequently the probability of contacting multiple nanowires for each device. In this design, we used three different effective channel widths of 480, 780, and 2600 μm, with fixed channel length of 2.5 μm. Typically one device of 780 μm channel width contains about 10 nanowires in the channel as shown in Figure 1c. The inset shows a magnified SEM image of one nanowire in the channel. The use of multiple nanowires per sensor offers high device yield (~70%) and small device-to-device variation (Figure S1). The above described procedure also allows for device fabrication on unconventional substrates, such as polyethylene terephthalate and glass. Moreover, biocompatible, FDA-approved materials such as parylene can be used as the substrate, allowing for in-vivo, flexible sensors.

The transistor properties of the devices were characterized, with the Si substrate as a back gate and 500 nm SiO_2 as a dielectric layer. Plots of drain-source (D-S) current (I_{ds}) *versus* D-S voltage (V_{ds}) under different gate voltage (V_g) for a typical transistor are shown in Figure 1d. The device exhibited a MOSFET like transistor behavior, and the linear regime can be well described by the conventional MOSFET equation (Eq.1, see also Figure S2);

$$I_{ds}=e\mu\varepsilon\varepsilon_r\frac{A}{d}\frac{V_{ds}}{L}(V_g - V_T)=g_m * (V_g - V_T)$$

(1)

where e is the elementary charge, μ is the device mobility, ε is the permitivity of vacuum, ε_r is the permitivity of SiO$_2$, A is the area of the channel, d is the spacing of the capacitor, L is the channel length, V_T is the threshold voltage, and g_m is the transconductance of the device. The linearity of I_{ds} at small V_{ds} confirms the negligible contact resistance. The on/off ratio of this device reached ~10^5. By carefully optimizing the density of NWs, we have demonstrated that about 70% of the devices showed an on/off ratio > 10^2. Only those were used in the following experiments.

Throughout this paper, we employed liquid gate measurements, in order to characterize and evaluate our devices under conditions as close as possible to the active sensing condition. This method was developed previously to gain insights on how biomolecules interact with sensors. [44] Our experimental setup for active measurements using the liquid gate configuration is schematically illustrated in Figure 1e. A device-under-test was fitted with a Teflon cell and the cell was then filled with 1 ml of phosphate buffered saline (PBS) solution. An Ag/AgCl reference electrode was inserted in the buffer that served as a liquid gate.[45] We confirmed that the leakage current is negligible compared to the current through the nanowires *via* control experiments (Figure S3 and ref. [44]).[46] For real-time biosensing experiments, after establishing a baseline, analyte solutions of interest were added to the buffer, and the change of the device characteristics was monitored over time. We note that for some of the measurements done below (Figure 1f, 2b, and 5a), continuous mixing of the buffer was performed by applying a constant continuous flow of air to the surface of the buffer solution in order to 1) minimize the mechanical/electrical perturbation to the system due to the addition of the analytes and 2) accelerate the mixing of the solutions.

We used streptavidin (S-Av) as the analyte and biotin as the receptor, since the system has been studied extensively.[47, 48] Biotin was attached to the nanowire surface through previously developed chemical procedure for our In$_2$O$_3$ nanowire biosensors.[4] A typical result of a real-time biosensing measurement is shown in Figure 1f, where three devices functionalized with biotin were exposed to a solution of 100 nM streptavidin at t = 100 s in 0.01× PBS. The change upon exposure, in terms of the absolute change in I_{ds} ($\varDelta I$), was 210, 95, and 35 nA for devices 2, 1, and 3, respectively. Clearly, there is a significant device-to-device variation.

Elucidation of Sensing Mechanism

We first investigated the physics leading to sensing signals for our In$_2$O$_3$ nanowire biosensors using biotin and streptavidin (S-Av) as a receptor/analyte model system. The change in the I_{ds}-V_g characteristics upon exposure to streptavidin (100 nM) was examined.[44] The experiment was carried out in 0.01× PBS. Figure 2a shows typical I_{ds}-V_g curves from a device before and after exposure to a solution of 100 nM streptavidin, where a clear difference was observed indicating successful sensing. The direction of the response is consistent with previous reports, which suggested that streptavidin contains amine base groups closer to the binding pocket, resulting in bringing positive charges close to the nanowires.[3, 49] We found that the change of the I_{ds}-V_g after the binding can be described as a parallel shift of the I_{ds}-V_g by ~14 mV (Figure S4). These observations were consistently reproduced over a large number of devices. Based on the observations, we attributed doping of nanowires by the analytes as the dominant sensing mechanism for In$_2$O$_3$ nanowire biosensors in the conditions used here, since under other possible mechanisms proposed before, such as change in dielectric constant and mobility, it must be accompanied with a change in the transconductance.[44, 50] We note that the observed shifts in the I_{ds}-V_g are not due to device instability over time or a perturbation caused by adding

a liquid, as verified by repeatedly measuring the I_{ds}-V_g and monitoring the change of on-current (I_{ds} at $V_g = 0.6$ V) over time. The change in I_{ds}-V_g curves was only observed with the introduction of streptavidin (Figure S5), while the current was stable before the introduction of streptavidin. We also note that there was no change when PBS was added to the solution. Furthermore, we have conducted a control experiment to confirm the binding of streptavidin, in which the nanowires with biotin were exposed to a solution of streptavidin tagged with 10 nm Au nanoparticles. The inset in Figure 2a is a typical SEM image of an In_2O_3 nanowire after the exposure, showing the binding of streptavidin molecules with the gold particles onto the nanowires.

The results described above show that "doping" is the dominant mechanism behind the generation of a sensing signal. Such doping can be classified into two categories: charge transfer[50] and electrostatic interaction.[44] The former depends on the alignment of the chemical potential between the analyte and the sensor[51] as well as on the charge transfer resistance.[52] In contrast, the electrostatic interaction does not require the direct transfer of carriers through the interface, and has a characteristic screening length (Debye length, λ_D) associated with the dielectric properties of the environment through which the electrostatic interaction takes place (buffer and In_2O_3 nanowire in our case).[53, 54] To establish which type of doping is at the origin of the sensing mechanism for our biosensors, the device response to 100 nM streptavidin was tested in buffers with three different electrolyte concentrations, thus different Debye lengths. Figure 2b shows I_{ds} *versus* time plots in 1× PBS (black, λ_D=0.7nm), 0.01× PBS (yellow, λ_D=7nm), and 0.0001x PBS (blue, λ_D=70nm), when the device was exposed to 100 nM streptavidin solution at t = 100 s. The extracted relative response is plotted *versus* ionic concentration in Figure 2c. The strong dependence of the responses to the ionic concentration indicates that the sensing is done by electrostatic interaction rather than charge transfer for our In_2O_3 nanowires.

Correlation between Transistor Performance and Biosensor Performance

Based on the device characteristics described above, we propose a metric to predict/calibrate the biosensor performance in terms of the absolute response (*ΔI*). The metric dI_{ds}/dV_g will correlate the absolute response (*ΔI*) with the change in effective gate voltage induced by binding of biomolecules. The correlation of dI_{ds}/dV_g to the device sensitivity was investigated as follows: I_{ds}-V_g measurements were performed on several devices using a liquid gate in 0.01× PBS, and dI_{ds}/dV_g determined at $V_{ds} = 200$ mV. The devices were then exposed to 100 nM streptavidin, and the I_{ds}-V_g measurement was performed again. The absolute response (*ΔI*) for each device was calculated, and correlated to dI_{ds}/dV_g by linear fitting. Data points at $V_g = 0.6$ V were used for the analysis here. Shown in Figure 3 is a plot of the absolute response *versus* dI_{ds}/dV_g with a linear fitting (black solid line) for five different devices. The fitting yielded a correlation coefficient of ~0.98, proving the solid correlation between those two values. We note that a similar analysis at different gate voltages also revealed consistent results. This correlation was used to calibrate the sensor responses as shown in the next section.

While it is not the main point of this paper, we note that the correlation can be also used to predict the behavior of a given transistor as a biosensor. As a consequence, a feedback loop can be used to design improved biosensors with shorter feedback time. In addition, the results indicate one can tune the magnitude of the response of a biosensor by applying an appropriate gate voltage to maximize the value of dI_{ds}/dV_g. In fact, the plot of dI_{ds}/dV_g *versus* the absolute response revealed a clear correlation between them, and the gate voltage that gives the maximum dI_{ds}/dV_g gives the maximum absolute response (Figure S6). Further discussions can be found in the supporting information.

Calibration of Sensor Response

The metric dI_{ds}/dV_g can be used to calibrate the sensor response. We have found that this calibration is achieved by dividing the absolute responses (ΔI) by dI_{ds}/dV_g, which is hereafter referred to as "calibrated response." As an example, Figure 4a shows absolute responses plotted against the device identification numbers together with an average of the responses before the calibration. By performing the calibration, we significantly reduce the device-to-device variation as shown in Figure 4b. The improvement was statistically verified by calculating the coefficient of variation (*CV*) for each set of data, where *CV* is defined as follows:

$$CV = \frac{\sigma}{\mu}$$

(2)

where σ is the standard deviation and μ is the mean. *CV* was reduced from 59% for the absolute response to 16% for the calibrated response, confirming the much reduced device-to-device variation after calibration. For comparison, we also performed the conventional normalization method, where the current/resistance/conductance was normalized by the initial value. The result is shown in Figure 4c. *CV* of the normalized response is 25%, which is slightly higher than that of calibrated response. This is as expected according to the analysis shown below.

We also performed the same calibration on the data shown in Figure 1d to show that the method works for real-time measurements. Figure 5 shows the plots of the resultant calibrated responses. It is clear that the large device-to-device variation observed in Figure 1d is significantly reduced by the calibration, confirming the applicability of our method to real-time biosensing. We note that the calibrated responses (change) of ~14 mV for the real-time measurement are consistent with the number observed for the I_{ds}-V_g measurement (~14 mV).

The physical meaning of this calibration is to translate the response (change) in current to responses (change) in voltage that is delivered by the analyte. This translation leads to an advantage of our calibration method compared to the conventional method where the change was normalized by the initial conductance/current/resistance, as shown below. Applying the conventional MOSFET model (Eq.1),[55] I_{ds} before/after the exposure to proteins can be expressed as follows:

$$I_{before} = e\mu_1\varepsilon\varepsilon_{r1}\frac{A}{d}\frac{V_{ds}}{L}(V_g - V_{T1})$$

(3a)

$$I_{after} = e\mu_2\varepsilon\varepsilon_{r2}\frac{A}{d}\frac{V_{ds}}{L}(V_g - V_{T2})$$

(3b)

where the characters with subscript 1 are for the parameters before exposure to biomolecules, and subscript 2 for the device after exposure to biomolecules. Our metric dI_{ds}/dV_g can be expressed as:

$$\frac{dI_{ds}}{dV_g} = e\mu_1\varepsilon\varepsilon_{r1}\frac{A}{d}\frac{V_{ds}}{L}$$

(4)

When electrostatic interaction is the dominant sensing mechanism, I_{after} can be written as:

$$I_{after}=e\mu_1\varepsilon\varepsilon_{r1}\frac{A}{d}\frac{V_{ds}}{L}(V_g - V_{T2})=e\mu_1\varepsilon\varepsilon_{r1}\frac{A}{d}\frac{V_{ds}}{L}(V_g - (V_{T1}+\Delta V)) \tag{5}$$

where ΔV is the equivalent gating voltage (potential) induced by the biomolecules. Using these equations, we can express the normalized response ($\Delta I/I_0$) as follows:

$$\frac{\Delta I}{I_0}=\left(\frac{e\mu_1\varepsilon\varepsilon_{r1}\frac{A}{d}\frac{V_{ds}}{L}(V_g - V_{T1}) - e\mu_1\varepsilon\varepsilon_{r1}\frac{A}{d}\frac{V_{ds}}{L}(V_g - (V_{T1}+\Delta V))}{e\mu_1\varepsilon\varepsilon_{r1}\frac{A}{d}\frac{V_{ds}}{L}(V_g - V_{T1})}\right)=\frac{\Delta V}{(V_g - V_{T1})} \tag{6a}$$

while the calibrated response ($\Delta I/(dI_{ds}/dV_g)$) can be expressed as follows:

$$\frac{\Delta I}{\frac{dI_{ds}}{dV_g}}=\left(\frac{e\mu_1\varepsilon\varepsilon_{r1}\frac{A}{d}\frac{V_{ds}}{L}(V_g - V_{T1}) - e\mu_1\varepsilon\varepsilon_{r1}\frac{A}{d}\frac{V_{ds}}{L}(V_g - (V_{T1}+\Delta V))}{e\mu_1\varepsilon\varepsilon_{r1}\frac{A}{d}\frac{V_{ds}}{L}}\right)=\Delta V \tag{6b}$$

As can be seen in the equations (6a and b), the normalized response is still affected by V_{T1}, which is subject to device-to-device variation. On the other hand, the calibrated response is no longer a function of the device performance, and it only depends on the equivalent gate potential induced by the biomolecules (ΔV). Therefore, our calibration method is superior to the conventional normalization since it excludes the device-to-device variation in terms of threshold voltage variation. Indeed, this was experimentally confirmed by us, as the normalized response showed larger CV (25%) than that of the calibrated responses (19%) as previously shown in Figure 4. Our method is a powerful tool for calibrating the sensor response of biosensors, especially for devices in which it is more challenging to get uniform V_T, such as carbon nanotube biosensors. We note that biosensing experiments are usually carried out with small V_{ds} (i.e., in the linear regime) to avoid electrochemical reaction which may be induced by large V_{ds}; however, the method works as long as I_{ds} is linearly dependent on V_g within small variation (equivalent ΔV induced by binding of biomolecules). Even for the saturation regime, while I_{ds} is proportional to V_g^2 over a large range, the I_{ds}-V_g within small variation of V_g can still be approximated with a linear curve.

Conclusions

In summary, we have performed a comprehensive study on In_2O_3 nanowire biosensors, and successfully developed a calibration method to reduce the device-to-device variation in the sensor responses. The method is based on a correlation we found between the absolute responses and the gate dependence of the biosensors measured by means of a liquid gate. Our study of the sensing mechanism of In_2O_3 nanowire biosensors using streptavidin as a model analyte first revealed that electrostatic interaction is the dominant sensing mechanism, similar to other nanowire biosensors (mostly based on silicon nanowires). Based on the sensing mechanism, we proposed that there is a strong correlation between the responses of the biosensors and gate dependence of the devices, and the correlation was confirmed experimentally. Lastly, using the correlation, we developed a data analysis method to calibrate the sensor performance by dividing the absolute response by the gate dependence of each device. Then we successfully reduced the device-to-device variation in the sensor response as verified by the reduced CV from 59% before the calibration to 19% after the calibration. We believe our method will be useful for other nanowire and nanotube FET-based sensor arrays, making multiplexed sensor arrays a practical solution for measuring/monitoring multiple analytes (biomarkers) simultaneously.

Method

In$_2$O$_3$ nanowires were grown on a Si/SiO$_2$ substrate using the laser ablation method and dispersed in isopropanol by sonication. The suspension of nanowires in isopropanol was dropped onto a Si/SiO$_2$ substrate, typically a 3″ wafer, generating a random distribution of nanowires, with roughly 1 nanwires per 100 μm^2. The thickness of the SiO$_2$ capping layer was 500 nm, unless otherwise stated. Following that was deposition of metal contacts using photolithography and lift-off technique. A bilayer of 10 nm Cr and 40 nm Au was used as the contact for our case.

Supplementary Material

Refer to Web version on PubMed Central for supplementary material.

Acknowledgments

References

1. Cui Y, Wei QQ, Park HK, Lieber CM. Nanowire Nanosensors for Highly Sensitive and Selective Detection of Biological and Chemical Species. Science 2001;293:1289–1292. [PubMed: 11509722]

2. Chen RJ, Bangsaruntip S, Drouvalakis KA, Kam NWS, Shim M, Li YM, Kim W, Utz PJ, Dai HJ. Noncovalent Functionalization of Carbon Nanotubes for Highly Specific Electronic Biosensors. Proc Natl Acad Sci USA 2003;100:4984–4989. [PubMed: 12697899]

3. Star A, Gabriel JCP, Bradley K, Gruner G. Electronic Detection of Specific Protein Binding Using Nanotube FET Devices. Nano Lett 2003;3:459–463.

4. Li C, Curreli M, Lin H, Lei B, Ishikawa FN, Datar R, Cote RJ, Thompson ME, Zhou CW. Complementary Detection of Prostate-Specific Antigen Using In$_2$O$_3$ Nanowires and Carbon Nanotubes. J Am Chem Soc 2005;127:12484–12485. [PubMed: 16144384]

5. Bunimovich YL, Shin YS, Yeo WS, Amori M, Kwong G, Heath JR. Quantitative Real-Time Measurements of DNA Hybridization with Alkylated Nonoxidized Silicon Nanowires in Electrolyte Solution. J Am Chem Soc 2006;128:16323–16331. [PubMed: 17165787]

6. Patolsky F, Zheng G, Lieber CM. Nanowire Sensors for Medicine and the Life Sciences. Nanomedicine 2006;1:51–65. [PubMed: 17716209]

7. Patolsky F, Zheng GF, Lieber CM. Nanowire-Based Biosensors. Anal Chem 2006;78:4260–4269. [PubMed: 16856252]

8. Star A, Tu E, Niemann J, Gabriel JCP, Joiner CS, Valcke C. Label-Free Detection of DNA Hybridization Using Carbon Nanotube Network Field-Effect Transistors. Proc Natl Acad Sci USA 2006;103:921–926. [PubMed: 16418278]

9. Stern E, Klemic JF, Routenberg DA, Wyrembak PN, Turner-Evans DB, Hamilton AD, LaVan DA, Fahmy TM, Reed MA. Label-Free Immunodetection with CMOS-Compatible Semiconducting Nanowires. Nature 2007;445:519–522. [PubMed: 17268465]

10. Curreli M, Zhang R, Ishikawa FN, Chang HK, Cote RJ, Zhou C, Thompson ME. Real-Time, Label-Free Detection of Biological Entities Using Nanowire-Based FETs. IEEE Trans Nanotechnol 2008;7:651–667.

11. Tang XW, Bansaruntip S, Nakayama N, Yenilmez E, Chang YL, Wang Q. Carbon Nanotube DNA Sensor and Sensing Mechanism. Nano Lett 2006;6:1632–1636. [PubMed: 16895348]

12. Abe M, Murata K, Kojima A, Ifuku Y, Shimizu M, Ataka T, Matsumoto K. Quantitative Detection of Protein Using a Top-Gate Carbon Nanotube Field Effect Transistor. J Phys Chem C 2007;111:8667–8670.

13. Zhang GJ, Zhang G, Chua JH, Chee RE, Wong EH, Agarwal A, Buddharaju KD, Singh N, Gao ZQ, Balasubramanian N. DNA Sensing by Silicon Nanowire: Charge Layer Distance Dependence. Nano Lett 2008;8:1066–1070. [PubMed: 18311939]

14. Kim A, Ah CS, Yu HY, Yang JH, Baek IB, Ahn CG, Park CW, Jun MS, Lee S. Ultrasensitive, Label-Free, and Real-Time Immunodetection Using Silicon Field-Effect Transistors. Appl Phys Lett 2007;91:103901–103903.

15. So HM, Park DW, Jeon EK, Kim YH, Kim BS, Lee CK, Choi SY, Kim SC, Chang H, Lee JO. Detection and Titer Estimation of Escherichia Coli Using Aptamer-Functionalized Single-Walled Carbon-Nanotube Field-Effect Transistors. Small 2008;4:197–201. [PubMed: 18214875]

16. Besteman K, Lee JO, Wiertz FGM, Heering HA, Dekker C. Enzyme-Coated Carbon Nanotubes as Single-Molecule Biosensors. Nano Lett 2003;3:727–730.

17. Patolsky F, Timko BP, Yu GH, Fang Y, Greytak AB, Zheng GF, Lieber CM. Detection, Stimulation, and Inhibition of Neuronal Signals with High-Density Nanowire Transistor Arrays. Science 2006;313:1100–1104. [PubMed: 16931757]

18. Stern E, Steenblock ER, Reed MA, Fahmy TM. Label-Free Electronic Detection of the Antigen-Specific T-Cell Immune Response. Nano Lett 2008;8:3310–3314. [PubMed: 18763834]

19. Wang CW, Pan CY, Wu HC, Shih PY, Tsai CC, Liao KT, Lu LL, Hsieh WH, Chen CD, Chen YT. In Situ Detection of Chromogranin a Released from Living Neurons with a Single-Walled Carbon-Nanotube Field-Effect Transistor. Small 2007;3:1350–1355. [PubMed: 17576645]

20. Jin S, Whang DM, McAlpine MC, Friedman RS, Wu Y, Lieber CM. Scalable Interconnection and Integration of Nanowire Devices without Registration. Nano Lett 2004;4:915–919.

21. Patolsky F, Zheng GF, Lieber CM. Fabrication of Silicon Nanowire Devices for Ultrasensitive, Label-Free, Real-Time Detection of Biological and Chemical Species. Nature Protocols 2006;1:1711–1724.

22. Smith PA, Nordquist CD, Jackson TN, Mayer TS, Martin BR, Mbindyo J, Mallouk TE. Electric-Field Assisted Assembly and Alignment of Metallic Nanowires. Appl Phys Lett 2000;77:1399–1401.

23. Huang Y, Duan XF, Wei QQ, Lieber CM. Directed Assembly of One-Dimensional Nanostructures into Functional Networks. Science 2001;291:630–633. [PubMed: 11158671]

24. Tao A, Kim F, Hess C, Goldberger J, He RR, Sun YG, Xia YN, Yang PD. Langmuir-Blodgett Silver Nanowire Monolayers for Molecular Sensing Using Surface-Enhanced Raman Spectroscopy. Nano Lett 2003;3:1229–1233.

25. Rao SG, Huang L, Setyawan W, Hong SH. Large-Scale Assembly of Carbon Nanotubes. Nature 2003;425:36–37. [PubMed: 12955130]

26. Kim Y, Minami N, Zhu WH, Kazaoui S, Azumi R, Matsumoto M. Langmuir-Blodgett Films of Single-Wall Carbon Nanotubes: Layer-by-Layer Deposition and in-Plane Orientation of Tubes. Jpn J Appl Phys 2003;42:7629–7634.

27. Tsukruk VV, Ko H, Peleshanko S. Nanotube Surface Arrays: Weaving, Bending, and Assembling on Patterned Silicon. Phys Rev Lett 2004;92:65502–65505.

28. Han S, Liu XL, Zhou CW. Template-Free Directional Growth of Single-Walled Carbon Nanotubes on a- and R-Plane Sapphire. J Am Chem Soc 2005;127:5294–5295. [PubMed: 15826147]

29. Kocabas C, Hur SH, Gaur A, Meitl MA, Shim M, Rogers JA. Guided Growth of Large-Scale, Horizontally Aligned Arrays of Single-Walled Carbon Nanotubes and Their Use in Thin-Film Transistors. Small 2005;1:1110–1116. [PubMed: 17193404]

30. Wang YH, Maspoch D, Zou SL, Schatz GC, Smalley RE, Mirkin CA. Controlling the Shape, Orientation, and Linkage of Carbon Nanotube Features with Nano Affinity Templates. Proc Natl Acad Sci USA 2006;103:2026–2031. [PubMed: 16461892]

31. Lee M, Im J, Lee BY, Myung S, Kang J, Huang L, Kwon YK, Hong S. Linker-Free Directed Assembly of High-Performance Integrated Devices Based on Nanotubes and Nanowires. Nature Nanotechnol 2006;1:66–71. [PubMed: 18654144]

32. Liu XL, Han S, Zhou CW. Novel Nanotube-on-Insulator (Noi) Approach toward Single-Walled Carbon Nanotube Devices. Nano Lett 2006;6:34–39. [PubMed: 16402783]

33. Yu GH, Cao AY, Lieber CM. Large-Area Blown Bubble Films of Aligned Nanowires and Carbon Nanotubes. Nature Nanotechnol 2007;2:372–377. [PubMed: 18654310]

34. Li XL, Zhang L, Wang XR, Shimoyama I, Sun XM, Seo WS, Dai HJ. Langmuir-Blodgett Assembly of Densely Aligned Single-Walled Carbon Nanotubes from Bulk Materials. J Am Chem Soc 2007;129:4890–4891. [PubMed: 17394327]

35. Fan ZY, Ho JC, Jacobson ZA, Razavi H, Javey A. Large-Scale, Heterogeneous Integration of Nanowire Arrays for Image Sensor Circuitry. Proc Natl Acad Sci USA 2008;105:11066–11070. [PubMed: 18685094]

36. Heo K, Cho E, Yang JE, Kim MH, Lee M, Lee BY, Kwon SG, Lee MS, Jo MH, Choi HJ, Hyeon T, Hong S. Large-Scale Assembly of Silicon Nanowire Network-Based Devices Using Conventional Microfabrication Facilities. Nano Lett 2008;8:4523–4527. [PubMed: 19367934]

37. Li MW, Bhiladvala RB, Morrow TJ, Sioss JA, Lew KK, Redwing JM, Keating CD, Mayer TS. Bottom-up Assembly of Large-Area Nanowire Resonator Arrays. Nature Nanotechnol 2008;3:88–92. [PubMed: 18654467]

38. Fan ZY, Ho JC, Jacobson ZA, Yerushalmi R, Alley RL, Razavi H, Javey A. Wafer-Scale Assembly of Highly Ordered Semiconductor Nanowire Arrays by Contact Printing. Nano Lett 2008;8:20–25. [PubMed: 17696563]

39. Monica AH, Papadakis SJ, Osiander R, Paranjape M. Wafer-Level Assembly of Carbon Nanotube Networks Using Dielectrophoresis. Nanotechnol 2008;19:85303–85307.

40. Agarwal A, Buddharaju K, Lao IK, Singh N, Balasubramanian N, Kwong DL. Silicon Nanowire Sensor Array Using Top-Down CMOS Technology. Sens Actuators, A 2008;145:207–213.

41. Abe M, Murata K, Ataka T, Matsumoto K. Calibration Method for a Carbon Nanotube Field-Effect Transistor Biosensor. Nanotechnol 2008;19:45505–45508.

42. Li C, Zhang D, Han S, Liu X, Tang T, Lei B, Liu Z, Zhou C. Synthesis, Electronic Properties, and Applications of Indium Oxide Nanowires. Molecular Electronics Iii 2003;1006:104–121.

43. Lei B, Li C, Zhang D, Tang T, Zhou C. Tuning Electronic Properties of In2o3 Nanowires by Doping Control. Appl Phys A 2004;79:439–442.

44. Heller I, Janssens AM, Mannik J, Minot ED, Lemay SG, Dekker C. Identifying the Mechanism of Biosensing with Carbon Nanotube Transistors. Nano Lett 2008;8:591–595. [PubMed: 18162002]

45. Minot ED, Janssens AM, Heller I, Heering HA, Dekker C, Lemay SG. Carbon Nanotube Biosensors: The Critical Role of the Reference Electrode. Appl Phys Lett 2007;91:93507–93509.

46. Ishikawa FN, Chang HK, Curreli M, Liao HI, Olson CA, Chen PC, Zhang R, Roberts RW, Sun R, Cote RJ, Thompson ME, Zhou C. Label-Free, Electrical Detection of the SARS Virus N-Protein with Nanowire Biosensors Utilizing Antibody Mimics as Capture Probes. ACS Nano 2009;3:1219–1224. [PubMed: 19422193]

47. Bayer EA, Benhur H, Wilchek M. Isolation and Properties of Streptavidin. Methods in Enzymology 1990;184:80–89. [PubMed: 2388598]

48. Green NM. Avidin and Streptavidin. Methods in Enzymology 1990;184:51–67. [PubMed: 2388586]

49. Bradley K, Briman M, Star A, Gruner G. Charge Transfer from Adsorbed Proteins. Nano Lett 2004;4:253–256.

50. Gruner G. Carbon Nanotube Transistors for Biosensing Applications. Anal Bioanal Chem 2006;384:322–335. [PubMed: 16132132]

51. Li C, Zhang DH, Lei B, Han S, Liu XL, Zhou CW. Surface Treatment and Doping Dependence of In2o3 Nanowires as Ammonia Sensors. J Phys Chem B 2003;107:12451–12455.

52. Chidsey CED. Free-Energy and Temperature-Dependence of Electron-Transfer at the Metal-Electrolyte Interface. Science 1991;251:919–922. [PubMed: 17847385]

53. Stern E, Wagner R, Sigworth FJ, Breaker R, Fahmy TM, Reed MA. Importance of the Debye Screening Length on Nanowire Field Effect Transistor Sensors. Nano Lett 2007;7:3405–3409. [PubMed: 17914853]

54. Nair PR, Alam MA. Screening-Limited Response of Nanobiosensors. Nano Lett 2008;8:1281–1285. [PubMed: 18386914]

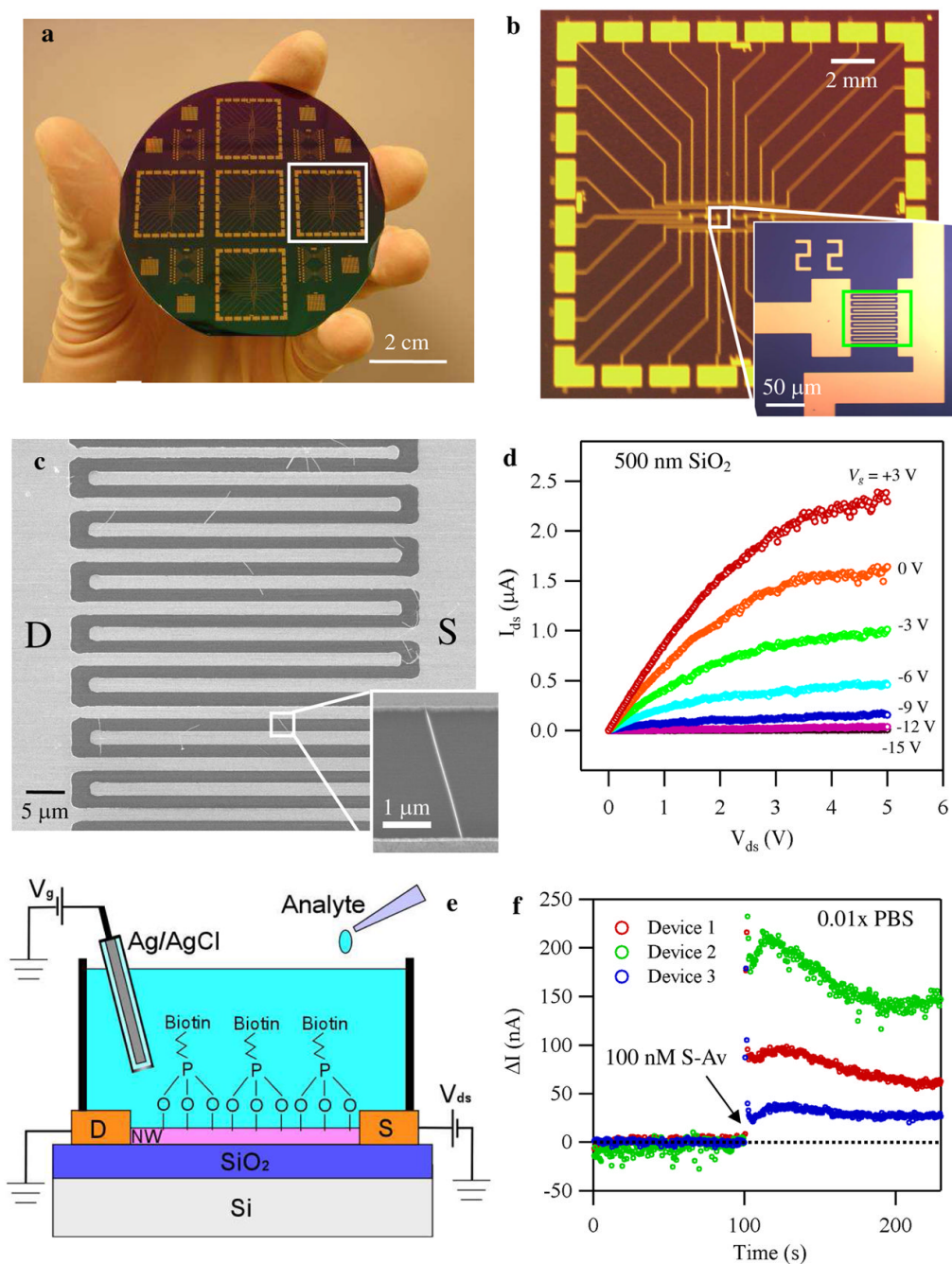55. Sze, SM. Semiconductor Devices: Physics and Technology. Vol. 2. Wiley; 2001.

Figure 1.
a) An optical micrograph of a 3″ wafer with multiple biosensor chips. b) A photograph of one chip with an inset showing an optical image of the interdigitated electrodes. c) A SEM image of multiple In_2O_3 nanowires between the source and drain electrodes. The inset is a magnified image of an individual nanowire. d) I_{ds}-V_{ds} plots under different V_g. e) Schematic diagram of the sensing setup illustrating an FET biosensor device operated by the liquid gate. f) Typical plots of the change in current *versus* time for three devices which were exposed to streptavidin (S-Av) of 100 nM at t = 100 s in 0.01× PBS. V_{ds} of 0.2 V and V_g of 0.6 V were used for the measurement.
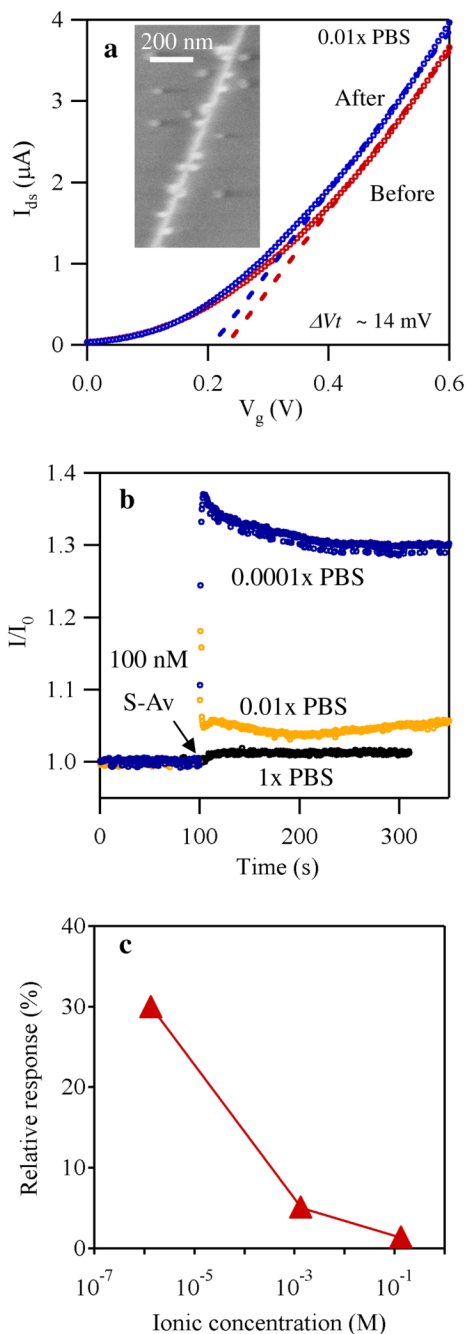
Figure 2.
a) I_{ds} *versus* V_g using the liquid gate before (red) and after (blue) exposure to streptavidin of 100 nM in 0.01× PBS. b) Plots of current *versus* time in PBS of different levels of dilution. The devices were exposed to 100 nM streptavidin at t = 100 s. V_{ds} of 0.2 V and V_g of 0.6 V were used for the measurement. c) Relative responses extracted from Figure 2b plotted against the logarithm of the ionic concentration.
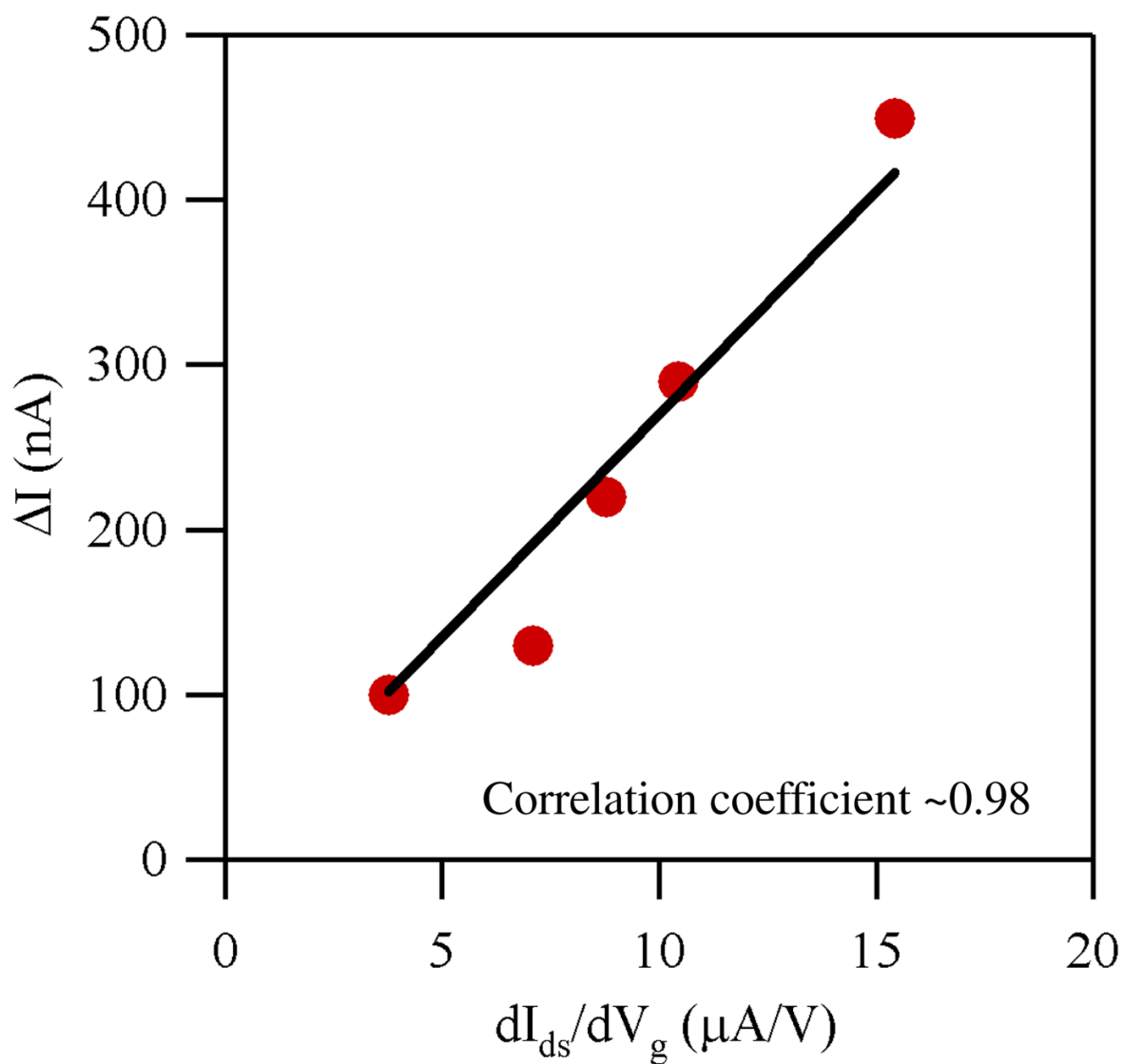
Figure 3.
Plots of absolute response *versus dI_ds/dV_g* for five devices. The solid line represents the fitting assuming a linear correlation, which yielded a correlation coefficient of ~0.98.
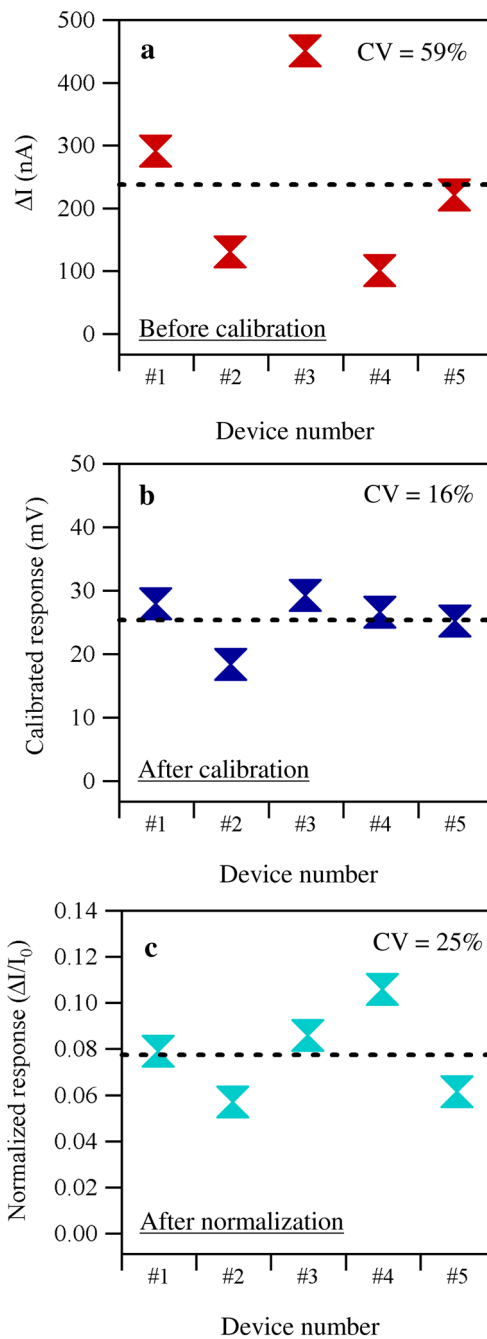
Figure 4.
a) Plots of the absolute responses for five devices *versus* the device identification number before the calibration. b) Same plots after the calibration. The vertical axis was switched to the calibrated response. c) Same plots after the conventional normalization. The vertical axis is the normalized response.
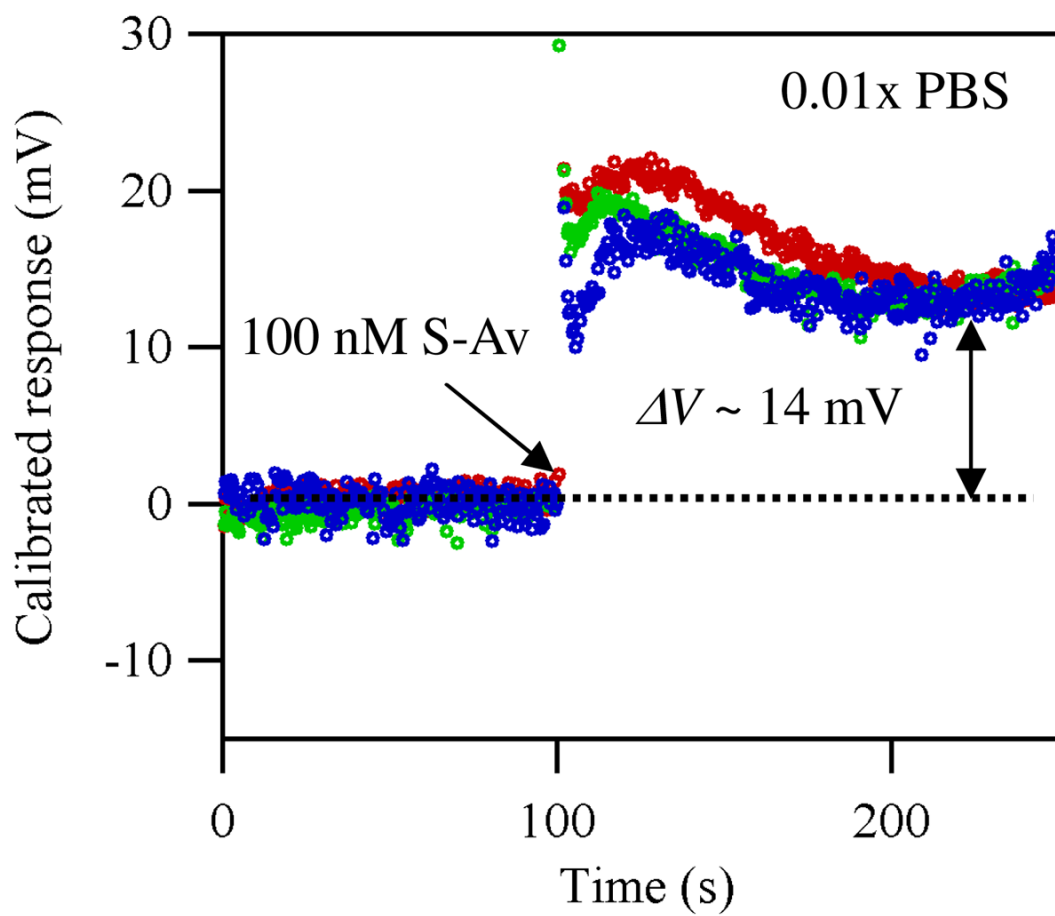
Figure 5.
Plots of the calibrated response using the data shown in Figure 1d.